Available online at www.sciencedirect.com

ScienceDirect

Procedia Engineering 2 (2010) 835–843

Procedia Engineering

www.elsevier.com/locate/procedia

Fatigue 2010

Fatigue properties of laser welded dual-phase steel joints

N. Farabi[a], D.L. Chen[a]*, Y. Zhou[b]

[a]*Department of Mechanical and Industrial Engineering, Ryerson University, 350 Victoria Street, Toronto, Ontario M5B 2K3, Canada*
[b]*Department of Mechanical and Mechatronics Engineering, University of Waterloo, 200 University Avenue West, Waterloo, Ontario N2L 3G1, Canada*

Received 17 February 2010; revised 10 March 2010; accepted 15 March 2010

Abstract

The aim of this study was to evaluate the effect of laser welding on fatigue properties of DP600 and DP980 steels in relation to the microstructural change and softening in the heat-affected zone. The degree of softening was found to be stronger in the DP980 welded joints than in the the DP600 welded joints. While the severity of the soft zone in the welded DP980 joints led to a significant decrease in the fatigue limit, the mild soft zone present in the DP600 welded joints had little or only a minor effect on the fatigue resistance. Despite the strong effect of the soft zone, the DP980 welded joints showed a similar or even longer fatigue life than that of both the DP600 welded joints and DP600 base metal at higher stress amplitudes. Fatigue crack initiation was observed to occur from the specimen surface, and crack propagation was characterized by the characteristic fatigue striations coupled with secondary cracks.

Keywords: Dual-phase steels; laser welding; microstructure; fatigue property; fractography.

1. Introduction

The constantly increasing environmental concerns regarding reducing CO_2 emissions and the drive of having better fuel economy have already motivated the car manufacturer to use the lighter weight materials having better mechanical properties. In terms of both mechanical properties and safety standards dual-phase (DP) steels have already built a reputation in the automobile industry. The microstructure of DP steels consists of islands of martensite in the ferrite matrix with or without the presence of retained austenite [1-4] where the martensite accounts for strength and the ferrite is responsible for ductility. Usually DP steels are produced by intercritical annealing followed by a rapid cooling [5,6]. During the intercritical annealing small pools of austenite are formed in the ferrite matrix, which subsequently transform into martensite upon rapid cooling. A hard and deformation-resistant phase is thus introduced into the microstructure during the austenite-to-martensite transformation and the accompanied volume expansion leads to the formation of mobile dislocations in the surrounding ferritic matrix. The mobility of these dislocations and their interactions with each other and with the grain/phase boundaries are responsible for the high initial work hardening rate and continuous deformation behavior in different grades of DP steels [6,7]. Therefore, compared with high strength low alloy (HSLA) steels, DP steels show a slightly lower yield

* Corresponding author. Tel: +1 416 979 5000 ext. 6487; fax: +1 416 979 5265. E-mail address: dchen@ryerson.ca (D.L. Chen).

1877-7058
doi:10.1016/j.proeng.2010.03.090

strength but a larger and more uniform total elongation, a higher initial work hardening rate in conjunction with a higher ultimate tensile strength.

The use of DP steels in the automotive applications unavoidably involves both the welding and joining in the manufacturing process and the fatigue resistance of welded joints due to the integrity and safety requirements. In terms of flexibility and ease of automation laser welding has already gained its popularity in the field of welding and joining. However, previous studies [3,8-10] showed that laser welding of DP steels led to the formation of a soft zone in the subcritical area of the heat-affected zone (HAZ) and the tensile properties of the welded joints were significantly influenced by the presence of such a soft zone. Then it is a matter of concern on how this soft zone manipulates the fatigue properties of laser welded DP steel joints. While a significant amount of work has been reported on the tensile properties of laser welded DP steel joints [8,11,12], the knowledge on the fatigue properties of this kind of joints is limited. As components of structural applications the laser welded DP steel joints with soft zones might be prone to failure under cyclic loading condition, it is necessary to characterize the fatigue resistance and fracture characteristics under cyclic loading. The present study was, therefore, aimed at evaluating the fatigue properties with emphasis on the failure mechanisms of the laser welded DP steel joints.

2. Materials and experimental procedure

The materials used in the present study were 1.2 mm thick DP600 steel sheet with a galvannealed coating (46 g/m^2 at the top and 47 g/m^2 at the bottom) and 1.2 mm thick DP980 steel sheet with a galvannealed coating (60 g/m^2 at the top and 67 g/m^2 at the bottom). The chemical composition of both DP steels is shown in Table 1. A Nuvonyx ISL4000L diode laser was used, with the selected welding parameters listed in Table 2. During welding ultra high purity argon was used as shielding gas at a flow rate of 16.5 l/min for DP600 steel and 14.2 l/min for DP980 steel with a welding speed of 1 m/min.

Table 1. The composition of dual-phase steels selected in the present study.

Steel grade	C	Mn	Si	Al	Mo	Cr	Cu	S	P
DP600	0.09	1.84	0.36	0.05	0.01	0.02	0.03	0.005	0.01
DP980	0.15	1.50	0.31	0.05	0.006	0.02	0.02	0.006	0.01

Table 2. Welding parameters selected in the present study.

Laser system	Laser source	Laser power (kW)	Welding speed (m/min)	Focal length (cm)	Beam dimension (mm^2)
Nuvonyx ISL-4000	Diode	4	1	9	12 × 0.9

The metallographic samples of the welded joints were cut perpendicular to the welding direction and were examined via a JSM-6380LV scanning electron microscope (SEM) coupled with energy dispersive X-ray spectroscopy (EDS) and 3D fractographic analysis. Vickers microindentation hardness tests were performed on the unetched samples with a load of 500 gm and a dwell time of 15 seconds. ASTM-E8M subsized specimens were used for the fatigue tests, and the geometry and dimensions of the fatigue test samples can be seen from Fig. 1 where the laser weld positioned at the center of gauge area was perpendicular to the loading direction. Fatigue tests were conducted using a fully computerized Instron 8801 servo-hydraulic testing system under load control and at more than 6 levels of stress amplitudes. A stress ratio of R ($\sigma_{min}/\sigma_{max}$) equal to 0.1, sinusoidal waveform and a frequency of 50 Hz were used in all tests. The fatigue fracture surfaces were examined using SEM to identify fatigue crack initiation sites and propagation mechanisms.

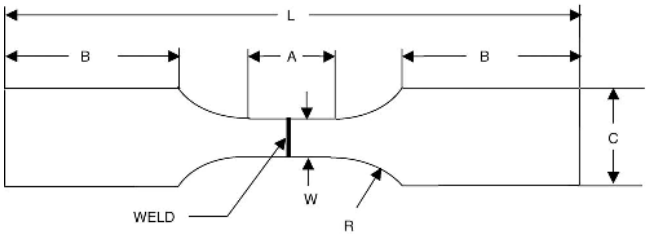

Name	L	A	W	R	B	C	Thickness
Dimension (mm)	140	32	6	6	~50	9.5	1.2

Fig. 1. Geometry and dimensions of the fatigue test specimens used in the present study.

3. Results and discussion

3.1. Microhardness and microstructural evolution

Fig. 2 shows the micro-indentation hardness profile of laser welded DP600 steel joints (Fig. 2(a)) and DP980 steel joints (Fig. 2(b)). The fusion zone (FZ) of DP600 welded joints showed significantly higher hardness values compared to the base metal. The SEM examinations of this region indicated that the microstructure in the FZ of DP600 joints was predominantly martensitic in conjunction with some sideplate ferrite and bainite (Fig. 3(a)). The variable hardness appeared in the FZ of DP600 welded joints would reflect the presence of such a multi-constituent microstructure. The formation of martensite in the FZ was a result of rapid cooling of the weld pool in the laser welding process.

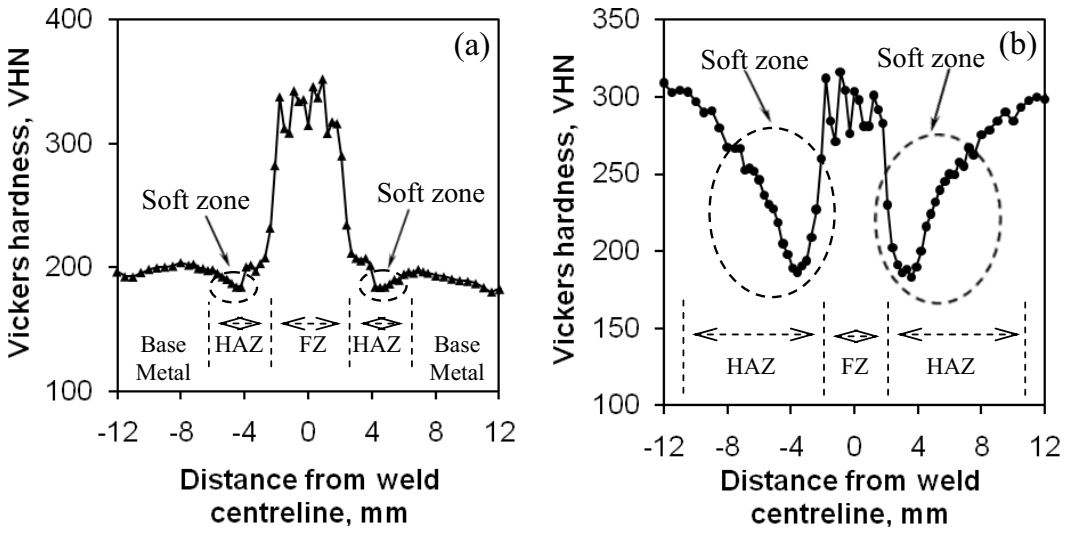

Fig. 2. Typical microhardness profile of the laser welded (a) DP600 steel joint and (b) DP980 steel joint.

It is seen from Fig. 2 that the hardness in the HAZ was lower than that in the base metal, which was called the soft zone as indicate in the figure. The presence of the soft zone in the HAZ of the DP600 welded joints (Fig. 2(a)) was mainly due to the tempering of pre-existing martensite [3,8,13] which corresponded the SEM image taken in

that area showing tempered martensite along with bainite in ferrite matrix (Fig. 3(b)). The hardness values in the base metal region of the DP600 welded joints were almost constant (Fig. 2(a)), since the microstructure (i.e., martensite in the ferrite matrix) in this region which was far from the center of FZ remained unaffected by the thermal cycle during laser welding, as shown in Fig. 3(c).

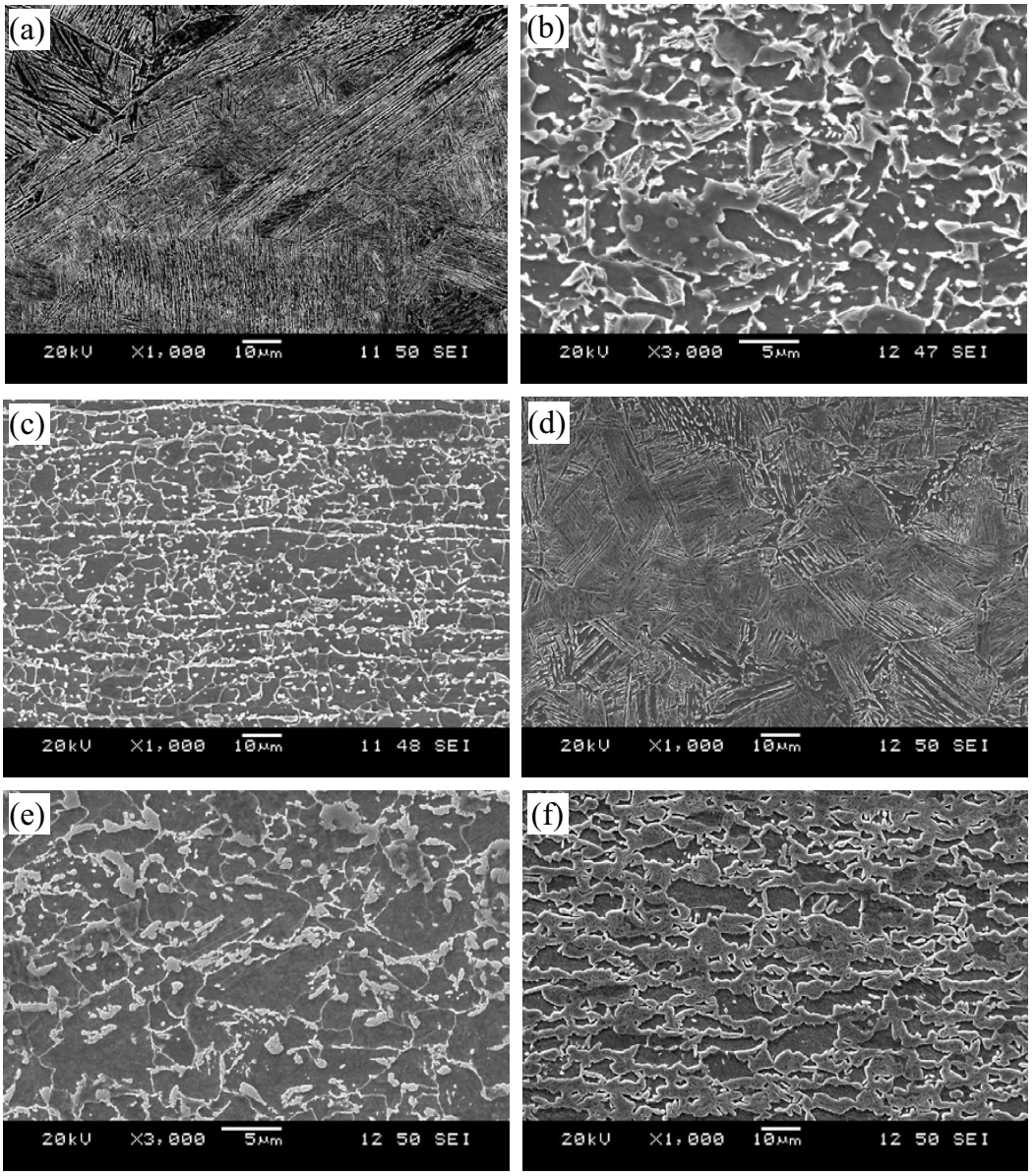

Fig. 3. SEM micrographs showing the microstructural change of laser welded DP steel joints, (a) DP600 fusion zone, (b) DP600 HAZ (soft zone), (c) DP600 base metal, (d) DP980 fusion zone, (e) DP980 HAZ (soft zone) and (f) DP980 base metal.

In contrast, the FZ of DP980 welded joints only showed a slight increase in the hardness values compared to the corresponding base metal (Fig. 2(b)) in spite of the formation of mostly martensitic microstructure in the FZ as well (Fig. 3(d)). This was due to the fact that more original martensite was already existent in the DP980 base metal (Fig. 3(f)) arising mainly from a higher amount of carbon content compared with the DP600 base metal (Table 1), thus giving rise to only a limited role of newly formed lath martensite in the FZ after laser welding. The quantitative image analysis indicated that the volume fraction of martensite was 0.25 in the DP600 base metal and 0.52 in the DP980 base metal, respectively, leading to a much higher hardness in the DP980 base metal (~300 HV) than that in the DP600 base metal (~190 HV), as shown in Fig. 2. However, the degree of softening was more severe and the size of the soft zone was larger in the case of DP980 welded joints than DP600 welded joints. This might be related to the following two possible reasons: First, the peak temperature experienced in the soft zone during laser welding seemed to cause partial disappearance of the pre-existent martensite, as seen in Fig. 3(e) showing the microstructure in the soft zone and Fig. 3(f) showing the microstructure in the DP980 base metal. It was likely that the peak temperature undergone in the soft zone could be high enough to promote either partial martensite-to-austenite solid-state transformation while the subsequent cooling phase might not cause the backward austenite-to-martensite solid-state transformation, or full martensite-to-austenite transformation in the heating phase and partial austenite-to-martensite transformation in the cooling phase, or both partial transformations in the heating and cooling phases during the welding thermal cycle. Apparently the occurrence of the microstructural changes depended on the location within the welded joint in view of the complexity of the temperature changes (magnitude, rate, and gradient, etc.). Further studies in this aspect are needed. Second, if there was no occurrence of the above-mentioned solid-state phase transformations, the presence of the higher amount of martensite in the DP980 steel would lead to a larger scale of tempering of pre-existing martensite in the HAZ, giving rise to greater and more severe softening in this material.

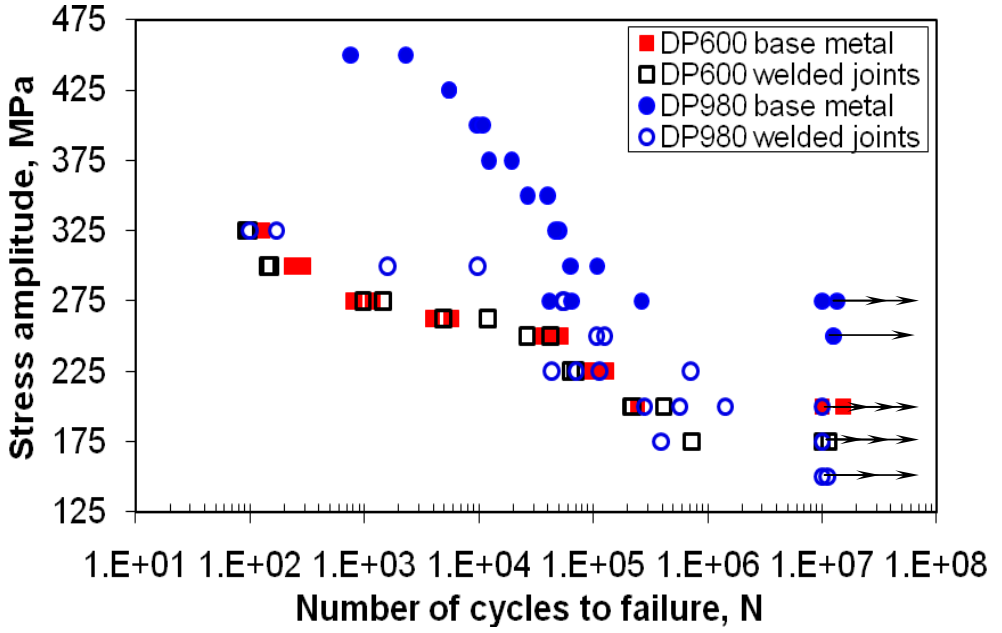

Fig. 4. S-N curves obtained for the base metals and laser welded joints of DP600 and DP980 steels tested at $R = 0.1$, 50 Hz and room temperature where the data points with arrow marks indicate the run-out samples.

3.2. Fatigue properties

The S-N curves obtained from the load control fatigue tests are shown in Fig. 4. The DP600 welded joints were found to have a slightly lower fatigue limit than that of the base metal. Indeed the DP600 base metal and the welded joints showed almost the same fatigue life within the experimental scatter at higher stress amplitudes.

This indicated that for the DP600 welded joints the slight drop in the hardness (Fig. 2(a)) in the HAZ was not large enough to reduce the fatigue strength at higher stress amplitudes, and thus the effect of laser welding on the fatigue resistance of DP600 steel could be negligible. On the other hand, DP980 welded joints showed a lower fatigue life than the DP980 base metal at both higher and lower stress amplitude levels. This corresponded well to the effect of the severe soft zone with a significant reduction in the hardness (Fig. 2(b)). Due to this significant softening in the HAZ the DP980 welded joints showed a considerably (~100 MPa) lower fatigue limit than the DP980 base metal. It should be noted that the softening in the DP980 welded joints was so severe that the lowest hardness in the soft zone was even slightly lower than that of DP600 welded joints (Fig. 2(a) and (b)), which also resembled to the findings from the fatigue tests (Fig. 4) where the DP980 welded joints showed even a fatigue limit lower than that of the DP600 welded joints. However, even though the negative effect of the soft zone on the fatigue resistance of the DP980 welded joints in comparison with the DP980 base metal was large, the fatigue life of the DP980 welded joints was basically longer than that of both the DP600 welded joints and DP600 base metal at the higher stress amplitudes (Fig. 4).

The obtained fatigue limit and fatigue ratio are tabulated in Table 3. The fatigue limit of the DP600 welded joints was 12.5% lower than that of the base metal, whereas the DP980 welded joints showed a 40% reduction in the fatigue limit compared to the base metal. The fatigue ratio of the DP600 welded joints and DP980 welded joints was obtained to be 0.28 and 0.21 respectively. All these results suggested that although the presence of the severe soft zone in the DP980 welded joints showed a detrimental effect, the mild soft zone present in the DP600 welded joints only exhibited a minor effect on the fatigue strength after laser welding.

Table 3. Fatigue limit and fatigue ratio of the base metals and laser welded joints of DP600 and DP980 steels tested at R = 0.1, 50 Hz and room temperature.

Material type	Fatigue limit (MPa)	Ultimate tensile strength (MPa)	Fatigue ratio
DP600 base metal	200	634	0.32
DP600 welded joints	175	630	0.28
DP980 base metal	250	1095	0.23
DP980 welded joints	150	724	0.21

Table 4. Fatigue parameters σ_f' and b for the base metals and laser welded joints of DP600 and DP980 steels tested at R = 0.1, 50 Hz and room temperature.

Material type	σ_f' (MPa)	b
DP600 base metal	415	-0.049
DP600 welded joints	435	-0.057
DP980 base metal	1019	-0.098
DP980 welded joints	472	-0.057

The obtained fatigue data plotted in Fig. 4 may be further fitted using the following Basquin type equation,

$$\sigma_a = \sigma_f^{'}(2N)^b, \tag{1}$$

where σ_a is the stress amplitude, $\sigma_f^{'}$ is the fatigue strength coefficient defined by the stress intercept at $2N$ =1, N is the number of cycle to failure and b is the fatigue strength exponent. The obtained values of $\sigma_f^{'}$ and b of the base metals and laser welded joints of DP600 and DP980 steels tested at R = 0.1, 50 Hz and room temperature are given in Table 4. Apparently the fatigue life at a given stress amplitude was dependent on both fatigue strength coefficient $\sigma_f^{'}$ and fatigue strength exponent b.

3.3. Fatigue failure location and mechanism

In all cases of fatigue tests the DP980 welded joints failed in the soft zone/HAZ, regardless of the stress amplitudes applied. Unlike the DP980 welded joints, the DP600 welded joints failed in the HAZ at the stress amplitudes above 250 MPa, but failed far away from the weld centreline or FZ at the stress amplitudes below 250 MPa. This distinct failure location was possibly due to the cyclic hardening mechanism involving deformation induced martensitic transformation [15-17]. The small amount of retained austenite existed in the DP steels transformed to martensite and gave additional strengthening effect during cyclic loading. These martensitic particles were considered to further pin the dislocations and dominate the deformation results [18]. In the low cycle fatigue (LCF) region, i.e., when the DP600 welded joints were tested at higher stress amplitudes, the dislocations could overcome these martensitic barriers; as the applied stress amplitude surpassed the pinning effect created by martensite a more cumulative damage occurred in the gauge section or in the HAZ in this case. But in the high cycle fatigue (HCF) region where the samples lasted for a longer period the applied stress amplitude was too low to overcome the pinning effect of the martensite and the area near the end of the gauge section became the weakest area due to potential stress concentration caused by the more or less notch effect. It was reported previously that the notch effect became stronger in the HCF region than the LCF region [19]. In contrast, in the case of DP980 welded joints the hardness reduction in the HAZ was so severe compared with the base metal (Fig. 2(b)) that the role of the deformation induced martensitic transformation would be masked. As a result, the soft zone in the HAZ directly represented the location of fatigue failure at all stress amplitudes. The fractographic examinations of the fracture surfaces revealed that fatigue crack initiation occurred from the specimen surface (Fig. 5(a) and (b)).

If there was no severe defects existent inside the material, fatigue crack initiation normally occurred from the specimen surface since the surface was usually less constrained than the interior grains [20]. The back and forth fine slip movement during cyclic loading built up notches or ridges at the surface (i.e., extrusions and intrusions) [14]. These kinds of notches with a notch root of atomic dimension could act as a stress riser and might act as the nucleation site of the fatigue crack. The fatigue crack could also result from the surface roughness. The samples tested at lower stress amplitudes showed the crack initiation from the surface along with a larger crack propagation area on the fracture surfaces. The crack propagation was mainly characterized by typical fatigue striations in conjunction with secondary cracks (Fig. 5(c)). These striations, usually perpendicular to the propagation direction, occurred by a repeated plastic blunting-sharpening process due to the slip of dislocations in the plastic zone at the fatigue crack tip [14,21]. The spacing between these striations was smaller near the crack initiation site and became larger with increasing distance from the crack initiation site since the striation spacing was associated with fatigue crack propagation rate. The faster crack propagation at the center of the left part of fracture surface in Fig. 5(a) was characterized by characteristic dimple rupture (Fig. 5(d)), representing typical ductile type of fracture mode. The slightly elongated oval shaped dimples due to shear motion were the primary feature near the edge of the fracture surface representing final rapid failure of the sample.

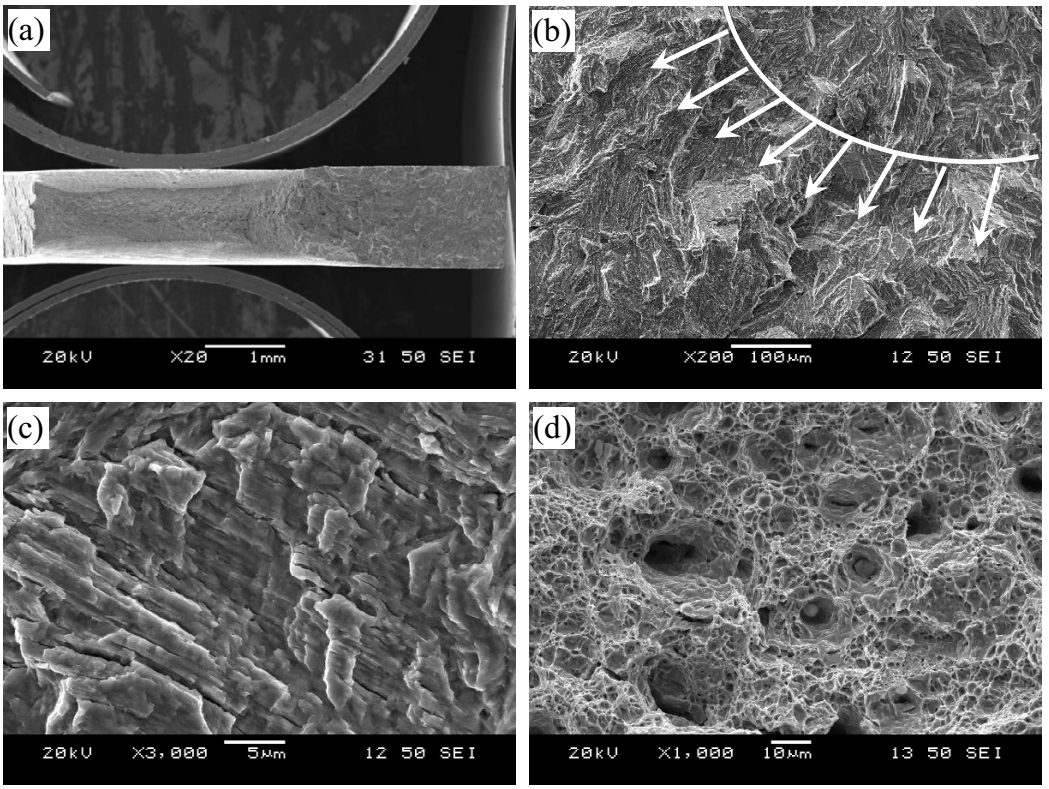

Fig. 5. Fatigue fracture surface of a DP980 welded joint tested at a stress amplitude of 225 MPa, (a) Overall view of the fracture surface at a low magnification, (b) crack initiation site, (c) crack propagation area, and (d) fast fracture area.

4. Conclusions

1. Rapid cooling of the weld pool in the laser welding process resulted in mostly lath martensitic structure in the fusion zone (FZ) which gave rise to higher hardness values significantly for DP600 steel and modestly for DP980 steel. A soft zone located in the heat-affected zone (HAZ) was observed. This was partly due to the occurrence of tempering of martensite pre-existent in the DP steels, and partly due to the disappearance of the original martensite in the form of solid state transformations caused by the high peak temperature experienced in the HAZ. The degree of softening was found to be more severe in the DP980 welded joints compared with the DP600 welded joints due to the higher volume fraction of martensite pre-existing in the DP980 base metal.

2. As a result of the presence of a severe soft zone the DP980 welded joints showed a significant decrease in the fatigue limit compared with the corresponding base metal. On the other hand, the presence of a mild soft zone in the DP600 welded joints were observed to have little or only a minor effect on the fatigue limit and fatigue life at higher stress amplitudes within the experimental scatter. However, even though the negative effect of the severe soft zone on the fatigue resistance of the DP980 welded joints was large, the fatigue life of the DP980 welded joints was still equivalent to or even longer than that of both the DP600 welded joints and DP600 base metal at higher stress amplitudes.

3. The DP980 welded joints failed exclusively in the soft zone, irrespective of the applied stress amplitudes. The DP600 welded joints failed in the soft zone at the stress amplitudes above 250 MPa, but failed in the base metal area at the stress amplitudes below 250 MPa. This distinct failure location appeared to be associated with deformation induced martensitic transformation.

4. Fatigue crack initiation was observed to occur from the specimen surface, and crack propagation was mainly characterized by the characteristic fatigue striations coupled with secondary cracks, with the striation spacing increasing with increasing distance from the crack initiation site.

Acknowledgements

The authors would like to thank the Natural Sciences and Engineering Research Council of Canada (NSERC), and Initiative for Automotive Innovation (Ontario Research Fund – Research Excellence) for providing financial support. N.F. thanks Ryerson School of Graduate Studies for his SGS scholarship. D.L.C. is also grateful for the financial support by the Premier's Research Excellence Award (PREA), Canada Foundation for Innovation (CFI), and Ryerson Research Chair (RRC) program. The authors would also like to thank J. Li (University of Waterloo) and Professor S.D. Bhole (Ryerson University) for their helpful discussion, and Messrs. A. Machin, Q. Li, J. Amankrah, D. Ostrom and R. Churaman for easy access to the laboratory facilities of Ryerson University and their assistance in the experiments.

References

[1] Bleck W. Cold-rolled high-strength sheet steels for auto applications. *JOM* 1996;**48**:26–30.

[2] Chen DL, Wang ZG, Jiang XX, Al SH, Shih CH. Dependence of near-threshold fatigue crack growth on microstructure and environment in dual-phase steels. *Mater Sci Eng A* 1989;**108**:141–51.

[3] Xia M, Biro E, Tian Z, Zhou YN. Effects of heat input and martensite on HAZ softening in laser welding of dual-phasesteels. *ISIJ Inter* 2008;**48**:809–14.

[4] Mediratta SR, Ramaswamy V, Singh V, Rama Rao P. Microstructure -mechanical property correlations in dual-phasesteels. *Trans Indian Inst Metals* 1985;**38**:350–72.

[5] Byun TS, Kim IS. Tensile properties and inhomogeneous deformation of ferrite-martensite dual-phase steels. *J Mater Sci* 1993;**28**: 2923–32.

[6] Davies RG. Influence of silicon and phosphorus on the mechanical properties of both ferrite and dual-phase steels. *Metall Trans A* 1979;**10**:113–18.

[7] Beynon ND, Oliver S, Jones TB, Fourlaris G. Tensile and work hardening properties of low carbon dual-phasestrip steels at high strain rates. *Mater Sci Tech* 2005;**21**:771–8.

[8] Xia M, Sreenivasan N, Lawson S, Zhou Y, Tian Z. A comparative study of formability of diode laser welds in DP980 and HSLA steels. *J Eng Mater Technol Trans ASME* 2007;**129**:446–52.

[9] Sreenivasan N, Xia M, Lawson S, Zhou Y. Effect of laser welding on formability of DP980 steel. *J Eng Mater Technol Trans ASME* 2008;**130**:0410041-0410049.

[10] Farabi N, Chen DL, Li J, Zhou Y, Dong SJ. Microstructure and mechanical properties of laser welded DP600 steel joints. *Mater Sci Eng A* 2010;**527**:1215–22.

[11] Larsson JK. Overview of joining technologies in the automotive industry. *Weld Res Abroad* 2003;**49**:29–45.

[12] Chung-Yun K, Tae-Kyo H, Bong-Keun L, Jeong-Kil K. Characteristics of Nd:YAG laser welded 600 MPa grade TRIP and DP steels. *Mater Sci Forum* 2007;**539-543**:3967–72.

[13] Xia MS, Kuntz ML, Tian ZL, Zhou Y, Failure study on laser welds of dual-phasesteel in formability testing. *Sci Tech Weld J* 2008;**13**:378–87.

[14] Dieter GE. *Mechanical Metallurgy*. SI ed. UK: Mcgraw-Hill; 1988.

[15] Hilditch TB, Timokhina IB, Robertson LT, Pereloma EV, Hodgson PD. Cyclic deformation of advanced high-strength steels: Mechanical behavior and microstructural analysis. *Metall Mater Trans A* 2009;**40**:342–53.

[16] Cheng X, Petrov R, Zhao L, Janssen M. Fatigue crack growth in TRIP steel under positive R-ratios. *Eng Fract Mech* 2008;**75**:739–49.

[17] Sugimoto K, Kobayashi M, Yasuki S. Cyclic deformation behavior of a transformation-induced plasticity-aided dual-phase steel. *Metall Mater Trans A* 1997;**28**:2637–44.

[18] Lukas P, Kunz L. Specific features of high-cycle and ultra-high-cycle fatigue. *Fatigue Fract Eng Mater Struct* 2002;**25**:747–53.

[19] Sauzay M, Gilormini P. Surface and cyclic microplasticity. *Fatigue Fract Eng Mater Struct* 2000;**23**:573–9.

[20] Chan KS, Yi-Ming P, Davidson D, McClung RC. Fatigue crack growth mechanisms in HSLA-80 steels. *Mater Sci Eng A* 1997;**222**:1–8.

[21] Laird C. Fatigue crack propagation. *ASTM STP* 1967;**415**:131–68.